JPhys Energy



# Observation of stimulated emission from Rhodamine 6G-polymer aggregate adsorbed at foam interfaces

JPhys Energy

PAPER

# Observation of stimulated emission from Rhodamine 6G-polymer aggregate adsorbed at foam interfaces

**Ketan Pancholi**[1,5], **Peter K J Robertson**[2,5], **Paul Okpozo**[1], **Neil S Beattie**[3] and **Dehong Huo**[4]

[1] School of Engineering, Sir Ian Wood Building, Robert Gordon University, Garthdee, Aberdeen, AB10 7QB, United Kingdom
[2] School of Chemistry and Chemical Engineering, Queen's University Belfast, Belfast, BT9 5AG. United Kingdom
[3] Department of Physics and Electrical Engineering, Northumbria University, Newcastle upon Tyne, NE1 8ST, United Kingdom
[4] School of Engineering, Newcastle University, Newcastle upon Tyne, NE1 7RU, United Kingdom
[5] Authors to whom any correspondence should be addressed.

**E-mail:** k.pancholi2@rgu.ac.uk **and** p.robertson@qub.ac.uk

**Keywords:** Stimulated emission, microbubbles, photocatalysis, interface, foam, lasing

Supplementary material for this article is available online

**OPEN ACCESS**

**RECEIVED**
5 July 2018

**REVISED**
19 October 2018

**ACCEPTED FOR PUBLICATION**
29 October 2018

**PUBLISHED**
11 December 2018



## Abstract

This paper reports for the first time the observation of stimulated emissions from the gas–liquid interface between two adjacent bubbles in highly ordered foams containing Rhodamine 6 G and surfactant. Stimulated emissions centred at 595 nm were observed when a monolayer of foam (~liquid fraction 0.11), placed on a highly reflective surface, was pumped with a 532 nm continuous wave laser directed along ~45° from the direction perpendicular to the substrate. Additionally, using confocal microscopy and micro-photoluminescence, it was found that the liquid fraction of the foam, the gap between two adjacent bubbles and the incidence angle of the laser are important parameters in guiding the light and promoting stimulated emissions at the interface. The adsorption of the polymer and dye increased the local concentration at the narrowest gaps between pairs of bubbles, which led to the formation of hemispherical micelles-dye agglomerates. The presence of the micelles aggregation caused random scattering induced stimulated emission. These results could have a significant impact on a number of applications, such as photocatalytic conversion at bubble interfaces, where $TiO_2$ can scatter light and hence reaction rates may be increased.

## 1. Introduction

Aggregation of the dye and nanoparticle materials are of great interest as a structure with potential applications in drug delivery measurement [1, 2], solar cells [3], sensors [4] and catalysis [5]. Aggregation, formed by an electrostatic, van der waals, $\pi$ interaction or hydrophilic effect, brings significant changes in optical and electronic properties of the structure [6]. For example, the controlled aggregation of $TiO_2$ nanocrystals brings substantial benefits to photocatalytic process. A study showed that the hydrogen production was found to be enhanced with the presence of $TiO_2$ nanoparticle agglomeration [7]. In hydrogen production, the multiple charges do not remain stored on the catalyst surface for long enough time for reaction to proceed. The charges are, however, easily stored in the confined spaced between $TiO_2$ nanoparticles in agglomerates and may then become available for reactions to proceed [8]. Moreover, the recombination of electrons with holes also slows down in agglomerates due to charge hopping between agglomerated nanoparticles [9]. The dye agglomerates also show similar nonlinear optical properties. The aggregates of Rhodamine 6 G dye adsorbed on amyloid protein fibres are found to produce the laser-like emissions through a random lasing process [10]. Such molecular complexes of dyes form the basis of biophotonics materials that is useful in improving diagnostic capabilities and other microlaser sensing applications [10].

Due to the simplicity and low cost, a range of materials such as semiconductors [11], quantum dots [12], nanoparticles [13, 14], liquid crystals [15, 16], and biological tissue [17] have been used to prepare the structures capable of producing a random lasing effect. A controlled manipulation of the metal–metal oxide

microstructure in hollow noble metal/ZnO core–shell nanoparticles can produce strong blue luminescence for increased photocatalytic activity [18]. Such structures have drawn great interst for nonlinear optical development also.

The random lasing occurs in an incoherent or coherent manner depending upon whether scattered light returns to its origin or not and the distribution of light is random in space and time [19]. The random scattering results an increased total photon path length [19]. When the photon path length becomes comparable to the De Broglie wavelength, the photons are localized to produce lasing with frequencies equivalent to the phase difference between backscattered waves [20]. The emission, however, is stimulated into long-lived spatial modes to achieve coherent or incoherent stimulation of emission at selected specific (resonant) frequencies [21]. Random lasing also occurs when light scatters off the dye agglomerates [22]. Depending upon their concentrations in aqueous solution, the hydrophobic interaction between dye and surfactant can result in J or H type of aggregates [23]. The maximum fluorescent emission from the aggregates is red-shifted compared to that of the monomer [24]. Changes in agglomerates size, shape and concentration can lead to a variety of emission changes [24].

By controlling agglomeration and assemblies, it is possible to create a structure that can produce desired nonlinear emission/absorbance responses [25]. Adsorption of nanoparticles, micelles or dye molecules at liquid–liquid or liquid–air interface allows creation of the desired nanoagglomerates [25]. The orientation of nanoparticles, dye molecules or micelles at interfaces experiences asymmetric forces causing anisotropic rearrangement which are significantly different than those occurring in the bulk phase [26]. Exploiting the interfaces of droplets and bubbles can allow formation of desired agglomerate structure.

Previously, Rhodamine 6 G was shown to propagate light at the interface between two neighbouring bubbles in foams with liquid fraction in the range of 0.04–0.2 [27]. At these liquid fractions, the probability of internal reflection of photons between two liquid films at the interface increases manifold to channelize the light. The weak scattering events, such as light diffusion, does not stimulate emission in foams. However, the formation of the dye aggregates due to increased local concentration of the dye-surfactant at the air–liquid interfaces stimulates the random lasing. Initially, the intensity of the emission increases linearly with the increase of the laser power excitation. When the system reaches its threshold, however, the emission intensity starts increasing rapidly at much higher rates in relation to the pumping power [28]. The adsorption of the polymer and Rhodamine 6 G molecules at the interface between two bubbles increases the disorder strength to achieve a degree of light localisation. The disorder strength was found to be maximum, where two adjacent bubbles are closest to each other [29]. A large gap, however, between two consecutive bubbles may have restricted stimulation as it does not efficiently adsorb the polymer at the interface causing diffusion [29].

In this study, it is shown that monolayers of dry foams of polyoxyethylene (40) stearate, containing Rhodamine 6 G (RD6G) and highly monodispersed sized bubbles, emit stimulated emissions at the interfaces between two neighbouring bubbles. The characteristics of the emissions depend on polymer and Rhodamine 6 G concentrations, foam liquid fraction and gap between two neighbouring bubbles.

## 2. Materials and methods

A spectroscopic grade of polyoxyethylene (40) stearate, ethanol, and Rhodamine 6G (RD6G) were purchased from Sigma-Aldrich and used without any further purification. Ultra-pure MiliQ de-ionised water with conductivity less than 18 Ω was used to prepare the solution. Stock solutions with 0.0025 wt% of polyoxyethylene (40) stearate were prepared by dissolving 7.5 mg of polymer in 300 ml of water. The solutions were sonicated for 15 min to fully dissolve the polymer in the water. Separately, an RD6G solution was prepared by dissolving 2 mg of dye in 1 ml of ethanol and stored in a clean vial. To prepare the bubbles, suitable amounts of both the polymer and the RD6G solutions were mixed together with water to obtain the desired dye concentration of 0.01 mM. The resulting solution was then passed through 0.2 $\mu$m filters to remove solid residues and free particles. The filtered solution had a refractive index of 1.42 and was used to prepare the bubbles as described in the next section.

### 2.1. Foam preparation

The bubbles were prepared by injecting the solution and $CO_2$ gas through a T-shaped device [30]. The required bubble diameter and the gap between two neighbouring bubbles were maintained by controlling the solution and carbon dioxide gas flow rates supplied to the device. An increasing $CO_2$ flow rate by keeping constant the flow rate of the solution resulted in an increased bubbles size and a decreased gap between neighbouring bubbles. By adjusting the flow rates, foams containing monodisperse sized bubbles with five different liquid fractions ranging from 0.09 to 0.4 were produced. The corresponding interfacial gaps between bubbles in the

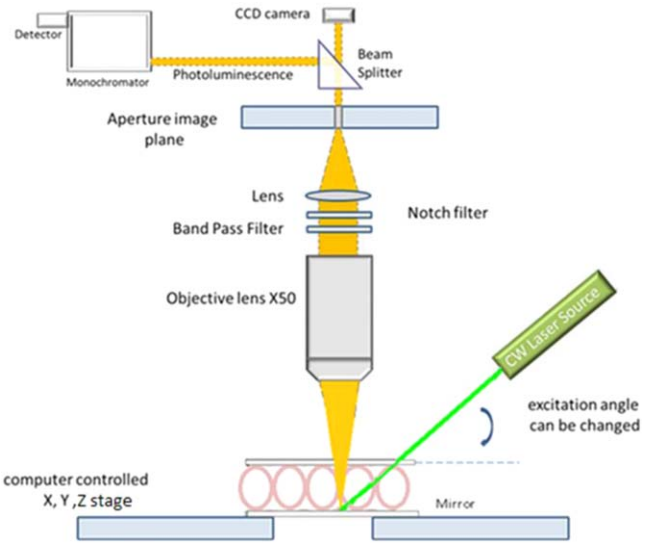


**Figure 1.** A scheme of the photo-luminescence measurement set-up.

prepared foams varied in the range 0.8–11 $\mu$m. The wettest foam contained uniform bubbles of 20 $\mu$m diameter whereas the driest foam contained bubbles of 250 $\mu$m.

For the optical characterisation, the foams were collected on 100 $\mu$m thick quartz slides (custom size 20 mm $\times$ 20 mm) and sandwiched by placing another quartz slide on the top. All sides of the was glued to confine the bubbles and allowing the formation of structured foam monolayers figure 3(a). The bubbles remained stable due to the positve pressure inside the structure. The described assemblage is referred to as 'flow cell' hereafter. It is worth mentioning that this arrangement stabilised the foams and restricted their movement. This allowed a consistent reproduction of the optical measurements conditions.

### 2.2. Photoluminescence spectroscopy

All spectra and spectral images were acquired using a micro-PL set-up as shown in figure 1. The monodisperse bubble foams were placed in the flow quartz cell (as explained in section 2.1) and excited with a continuous wave (CW) source of 532 nm argon-ion laser passed through a dichroic filter. The laser was focused on a spot with a diameter $<$1 mm at a grazing angle of $\sim$45° from the direction perpendicular to the quartz cell base (figure 1). The flow cells were placed on a mirror with 99.9% reflectivity to increase reflection. A variable neutral density filter was used to adjust the incident laser power. The emission signals collected from the top of the foams and the pumping beam axis were kept spatially separate using a six-axis stage to separate the transmitted pump beam from the signal.

The emitted signals from the bubble foams were collected through 20$\times$ (N.A.0.4) or 50$\times$ (N.A.0.75) objectives and focused onto a Princeton ICCD kinetic spectrometer (EPSRC loan pool) using an optical fibre. Real-time images of the foams illuminated with white light were obtained using a camera. Moreover, a shutter blocked the the pump beam at all times except during the exposure periods of the ICCD camera. The data were collected and analysed using a customized algorithm written in MATLAB. A reference spectrum from a solution without bubbles was also acquired to confirm whether the presence of micelles in the solutions produced stimulated emissions.

The intensity of light was measured by analysing the images using MATLAB. The reference intensity for calibration was derived from the images of a light source with a known intensity. A background signal was subtracted from each image before measuring the intensity. All images and measurements were obtained in a dark room with no background lights. Sufficient care was taken to ensure reproducible experimental protocols and image analysis in all measurements.

### 2.3. Time resolved measurements

The lifetime data were acquired using a HORIBA Scientific DeltaFlex fluorescence lifetime system equipped with a PPD detector and DeltaDiode DD-532LN (532 nm) excitation sources. The lifetime measurements, involved measuring the fluorescence decay for a set data collection time at a particular wavelength. Kinetic time-correlated single photon counting (TCSPC) measurements were made using the DeltaFlex with the DeltaDiode excitation source operated at 100 MHz. In this mode, the minimum collection period can be as low as 1 ms and up to 10 000 sequential decays can be acquired, along with the instrumental response in order to perform

reconvolution analysis. The datasets obtained were analysed in a batch mode using DAS6 software employing a multi-exponential model. From analysis of these data, the intensity (total counts in decay) and the average lifetime were returned. The quartz slide containing foam sample were positioned on motorised polarisers (magic angle condition) to minimise the scattering.

### 2.4. Confocal microscopy

Confocal microscopy was carried out to obtain images using a Nikon A1R (Invert), a fully motorized point scanning confocal microscope with hardware-enabled focus corrections. The system consisted of three photomultipliers each for fluorescence imaging, transmitted light detection and a dedicated photomultiplier array for spectral profiling. The resonant (fast scanning) and non-resonant (conventional scanning) scanning mirrors were both incorporated into the confocal scan-head. This allows imaging with high resolution (up to 4096 $\times$ 4096 pixels) and high speed (420 fps at 512 $\times$ 32 pixels). The bubbles confined in the flow cell were excited by the CW source of 532 nm argon-ion laser passed through a dichroic filter. Similar protocols to photoluminescence measurements were followed to collect the emission through a 20$\times$ (N.A.0.4) objective, which resulted in a series of 31 spectral images (1024 $\times$ 1024 pixels). A 50$\times$ (N.A.0.75) objective was used for measuring the gap between two adjacent microbubbles. The intensity of the light emitted from the interface between two bubbles was captured and then analysed using an image analysis software (Image J).

## 3. Results and discussion

Initially, when the laser beam was focussed on the bubble foams, it appeared opaque due to the scattering of the laser light. The interfaces between two adjacent bubbles, however, started appearing brighter in foam monolayers with liquid fraction between 0.09 and 0.17. This is evident in the half symmetrical 3D image of a foam (figure 2(a)), where the interfacial gaps containing liquid appear brighter than the rest of the foam. The conical shape visible in the 3D confocal image represents the interface between two adjacent bubbles. When two spherical objects are placed in an array, they form an interfacial gap of conical shape, which is illustrated in figure 2(b). A similar observation was also made in the two-dimensional confocal images, where the interfaces between adjacent bubbles appeared brighter than rest of the foam, as shown in figure 2(c). It should be noted that the measured values represented the gap appearing on the transverse image plane. Since the cross section of the interface was similar to a concave lens (figure 2(b)), the interface would be widest at the top surface; therefore, the gap between two adjacent bubbles decreases on moving through the thickness of the foam. Before acquiring spectra from the monolayer of the bubbles, the emission spectra were acquired from the bulk soluiton of the Rhodamine 6 G and surfactant.

### 3.1. Effect of foam liquid fraction in conducting light at interfaces

The appearance of bright interfaces between bubbles was only observed in foams with liquid fractions in range of 0.09–0.17. This confirms that light conducts efficiently through interfaces when the inverse of the liquid fraction in the foam is higher than the ratio between the photon transport mean free path and the absorption length scale of the solution [31]. The increased absorbance, combined with a contrast between the refractive index of the gas core and the water film ($\eta = 1.42$), channels photons in the liquid stored in the interface. Therefore, light propagation with a high capture fraction of 16% at the interface between two bubbles can be explained by total internal reflection [32]. To capture the maximum amount of light at the interface in subsequent characterisation experiments, a foam with 0.11 liquid fraction was used.

### 3.2. Stimulated emission

Figure 3(a) shows an example of a highly ordered monodispersed sized bubble foam used in the experiments. The excitation power of the 532 nm laser on the monolayer of RD6G-doped self-assembled bubble foam was gradually increased until it reached 65 mW. While increasing the power, the fluorescent emission spectra from the interface between two adjacent bubbles were also acquired for stimulated emission studies. Upon an initial increase of the excitation power, the foam started to change colour from bright yellow to orange, and several peaks of spontaneous emission appeared in the spectrum. The spectra were collected when all the peaks were stabilised. When the laser excitation power reached 31 mW, the orange yellow glow, localised at the interface between two neighbouring bubbles, appeared brighter (figure 3(b)). The collected emission spectra are shown in figure 4.

As can be seen in figure 4, when the excitation power reached a threshold of 5 mW, the intensity of the peak at 595 nm sharply increased and the full-width at half-maximum (FWHM) decreased to 10 nm. Additionally, a shoulder at 576 nm with 17 nm FWHM was also observed. Apart from these two peaks, the spectra also show relatively broad emissions in the range 530–590 nm which reflect the typical fluorescence of RD6G in water. The

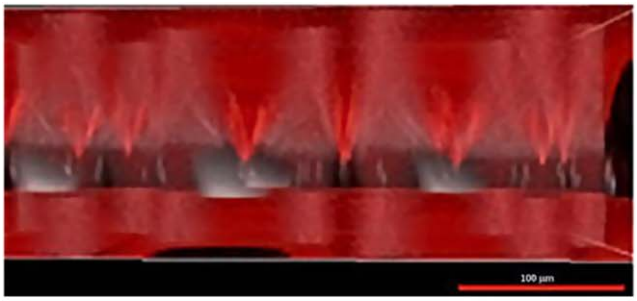


(a)

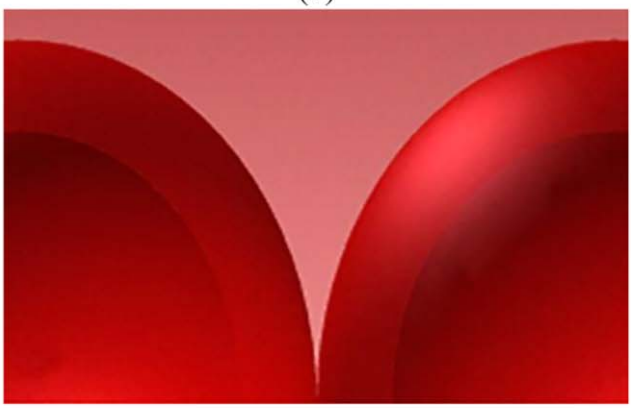

(b)

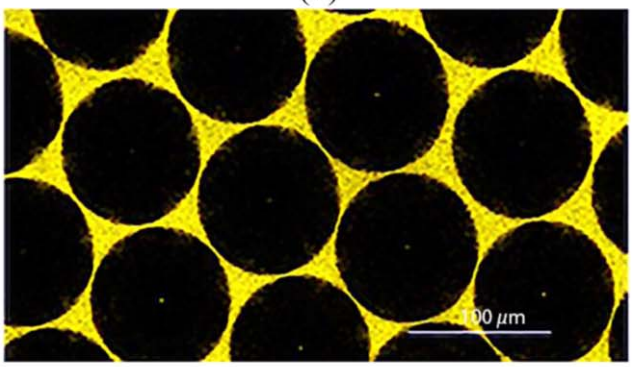


(c)

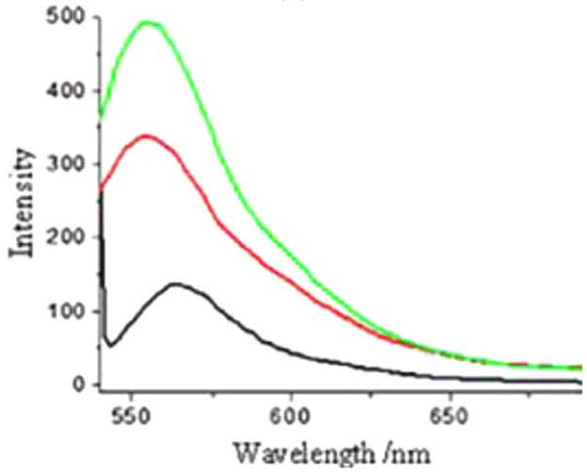


(d)

**Figure 2.** (a) A 3D image acquired using confocal microscopy shows a similar 3D cone appearing bright, while the bubbles appeared as voids between these triangles. Since the image only captures half symmetry, the other side of the cone does not appear. The light was conducted by the liquid around the bubble, which captured 16% of the transmitted light. (b) A two-dimensional image illustrates how a triangular conical gap is formed between two adjacent bubbles. (c) A 2D confocal image showing bright interfaces between bubbles confirms light capture. (d) The PL emission spectra obtained from the Rhodamine 6 G and surfactant solution showing peaks centred at 567, 563 and 562 nm with a full width at half-maximum (FWHM) of 30, 28 and 27 nm respectively. The RD6G doped foam was excited with 10 , 17 and 20 mW pumping energy.

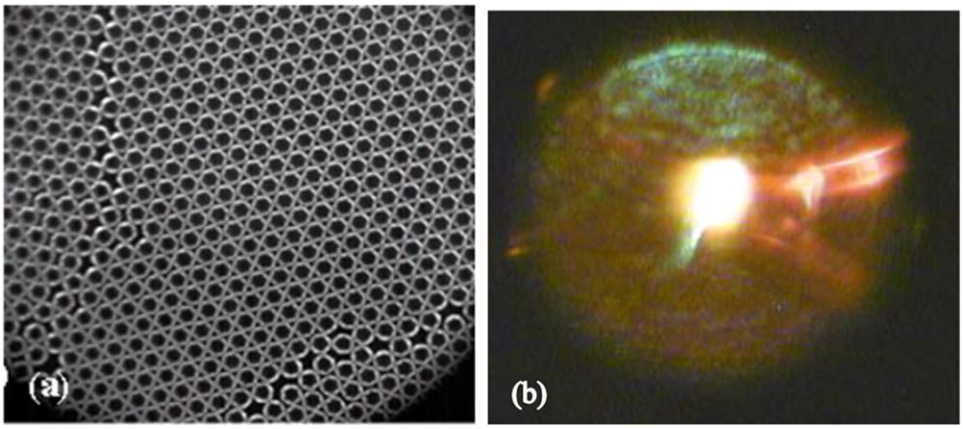


**Figure 3.** (a) An image showing a monolayer of monodisperse bubbles used in the current study, (b) an image of the interface between two bubbles showing lasing, when excited with 532 nm. Scale bar represents 100 micrometer.

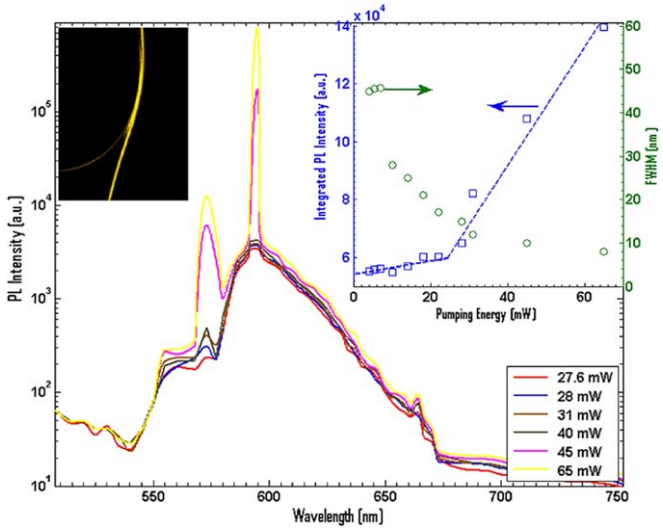


**Figure 4.** Fluorescent emission intensity spectra acquired from the interface of two adjacent bubbles at varying pumping power. The inset PL image shows the orange–yellow colour corresponding to the stimulated emission peak at 595 nm, while the inset plot shows the increase in the integrated PL intensity in response to variation in laser pumping power. The nonlinear behaviour explains the presence of the stimulated emission.

additional features detected in the range 600–760 nm are similar to the fluorescent emissions of RD6G dissolved in an aqueous amphiphilic surfactant solution shown in figure 2(d). The integrated fluorescent intensity of all spectra linearly increased with the excitation energy until a threshold value. Above the threshold, the PL integrated intensity increased with a much higher gradient at 595 nm (see inset of figure 4). With a further increase of the excitation power above the threshold, the amplitude of the peak increased without the appearance of resonant modes, which would otherwise be observed in Fabry–Perot cavity resonators. No mode spacing was observed confirming the absence of cavity mode of emission.

All spectra in figure 4 are red-shifted by approximately 30 nm compared to the fluorescence emission spectra from the Rhodamine 6G-PEG 40 S solution (figure 2(d)); this suggests the formation of J or H types of aggregates [26, 33]. It is well known that the cationic Rhodamine 6 G dye forms agglomerates in aqueous solution because of its hydrophobic interaction with water [34]. The addition of an amphiphilic surfactant below the critical micelles concentration (CMC), however, disperses the aggregates, forming a monomer-dye solution, which increases the fluorescence emission intensity [35].

Since polyoxyethylene 40 stearate concentration of 0.0075 wt% in solution was lower than the CMC (0.01 wt%) [36], the micelles, and subsequently the aggregates, must not have formed in the dye solution. It is well known that the micelles capture the dye from its centre leading to dye aggregation in solution [36]. In this experiment, however, the presence of phase boundaries between adjacent bubbles in the foams increased the local concentration of dye and surfactant molecules, leading to the reorientation of hydrophobic tails and

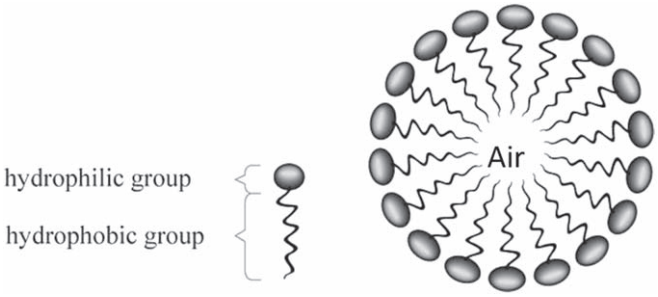


**Figure 5.** Surfactant molecules orientation around bubble.

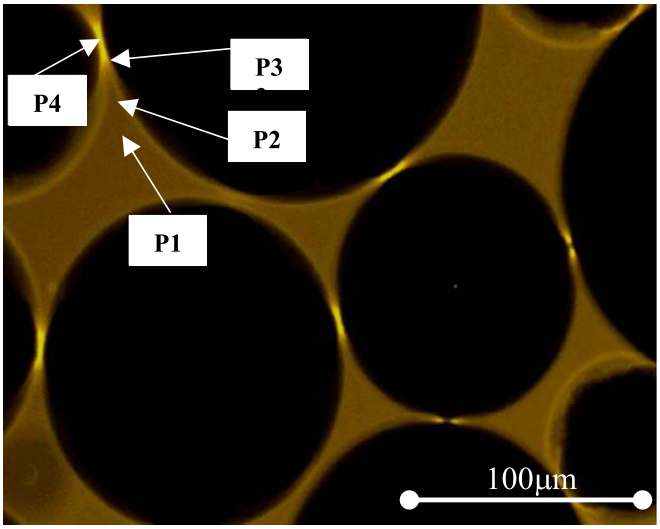


**Figure 6.** The fluorescence emission amplification observed at the interface with a gap of approximately 1 $\mu$m between two adjacent bubbles. When the gap is larger than 1 $\mu$m, the emission amplification at the interface is not observed. The spectra corresponding to the approximate spatial locations P1, P2, P3 and P4 are shown in figure 7.

hydrophilic heads of the micelles at the interfaces between bubbles, as previously reported [37, 38]. The hydrophobic tails remained oriented towards air, while the hydrophilic heads were located on the water side (figure 5) [39]. Such orientation determined repulsion between highly charged hydrophilic tails, allowing the local formation of hemispherical pre-micelle structures [40], which could have helped to capture the cationic dye in hydrophobic centres to form J or H aggregates at the interface between two bubbles [41]. The red-shifted fluorescence emission at 595 nm can be attributed to the presence of pre-micelle structures and Rhodamine 6 G intercalated by J type aggregates [42]. The red-shift in the emission results from the interactions between the dye monomers and increased cationic charge of high local dye-micelles concentrations or from weakly-coupled aggregates [43].

As visible in figure 6 (location P4 for instance), stimulated emissions are only observed when the gap between two adjacent bubbles is not larger than 1 $\mu$m. When the gap between two phase boundaries (in adjacent bubbles) is equal or less than 1 $\mu$m, the local concentration of agglomerates is maximized at the interfaces; this is in agreement with previous studies reporting that if the gap between two adjacent bubbles is less than twice the size of the aggregates, the local concentration of disordered agglomerates becomes high [41]. Additionally, the monolayer used in this work is a two-dimensional foam and therefore, the thin film between two bubbles forms a network that allows a random walk of photons [44, 45]. The diffusive random walk of photons is a weak scattering event and alone does not generate stimulated emissions [44]; however, the dye-surfactant agglomerates coupled with diffusive random walk increases residence time of the pohoton providing random feedback [45]. The area where the gap between two bubbles is larger than 1 $\mu$m does not show any increased intensity (figure 6) and therefore, it indicates absence of agglomerates as adsorbtion of the dye would be less between two bubbles [46]. If bubbles are near the dye molecule adsorbtion would increase and dye monomer will not long be present. It is worth noting that the incidence angle of the laser is important in achieving lasing. If

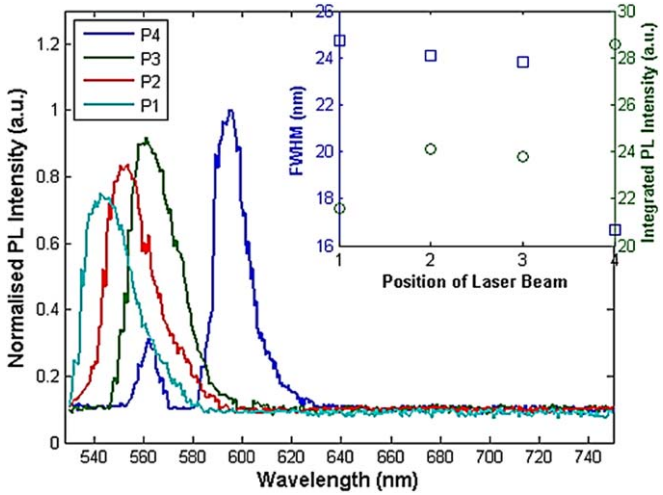


**Figure 7.** The plot shows spectra of the normalised fluorescence emission from four locations as shown in figure 6. The inset plot shows the integrated photoluminescence intensity for each spectrum referring to various spatial locations on the foam. Maximum standard error for all FWHM value is $\pm 0.72$. (All spectra are not shown.)

angle is not 45° and does not allows the light to propagate along the interface between two bubbles, the efficiency of light guide drops with the absence of diffsive random walk.

Since the shape, size, geometry of agglomerates and inter-agglomerate distance is related to the wavelength of the stimulated emission, signals from four different locations were collected and plotted in figure 6. The inter-agglomerate distance in the ensemble is determined by the balance of the capillary force and the long-range repulsion between two agglomerates [47].

Therefore, the force balance at the interface dictates that the local concentration of the agglomerates is maximum at P4 compared to other locations, such as P1, P2 and P3. The spectra acquired from the four locations showed similar trends. Moving away from the narrowest gaps (from location P4 to P1), the local concentration of dye decreases and results in in monomeric solution. The low dye concentration inhibits the formation of agglomerats. As seen in figure 7, the presence of agglomerates increases intensity but a red-shift of is also observed in relation to peak from monomeric solution (bulk solution, P4 location). With increase in solute concentration, the emission spectrum shifts towards the lower frequencies [33].

The side-band at 576 nm is related to the size, shape and concentration of the agglomerates. Additionally, a higher concentration of dye increases the capacity to absorb at shorter wavelengths and decreases the ratio between the absorbance at the main band and that at the side-band [43]. Agglomerates of small size, which are not intercalated with the surfactant, broadened the emission band and a blue-shift to 576 nm was also observed.

## 4. Morphology of dye agglomerates at interface

To investigate the morphology of the dye agglomerates around the bubbles in foam, the foam samples prepared as described previously. Samples were freeze dried on the TEM grid with membrane (300 $\mu$m grid size) before imaging. The TEM images, as seen in figure 8, show the formation of dye nanoagglomerates (figure 8(a)) around the bubble (figure 8(b)). The micelle with dye agglomerates and the slender side-to-side agglomerate formation are also observed in figures 8(c) and (d), respectively.

## 5. Time correlated single photon counting

The dye aggregation is known to responsible for short fuorescnce lifetime and self-quenching.[48] The TCSPC is used to study the dynamic processes through stimulated emission in such system. The excited state dynamics of Rhodamine 6 G aggregates and the influence of the bubble interface were investigated. The emission decay curves (figure 9) for a bulk solution of 0.01 mM concentration and a monolayer of bubbles prepared with same concentration (0.01 mM) were collected at 560 nm.

In comparison to a single exponential parameter fitting to decay curve for the bulk liquid, the emission decay curve from the monolayer of the bubbles were found to fit to the triple exponential parameter, which highlights

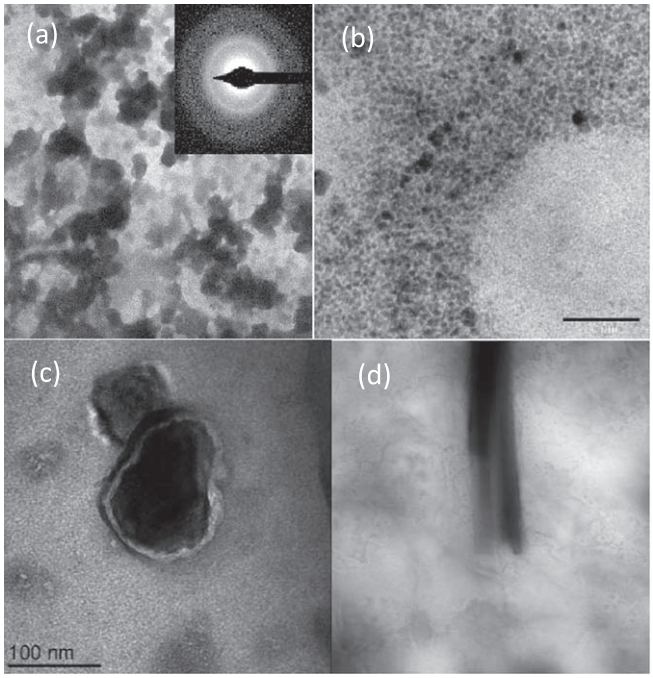


**Figure 8.** The TEM image of (a) Rhodamine 6 g agglomerated crystals (inset diffraction pattern) (b) dye agglomerate around bubble (c) micelle-dye crystal (d) slander structure of the agglomerate.

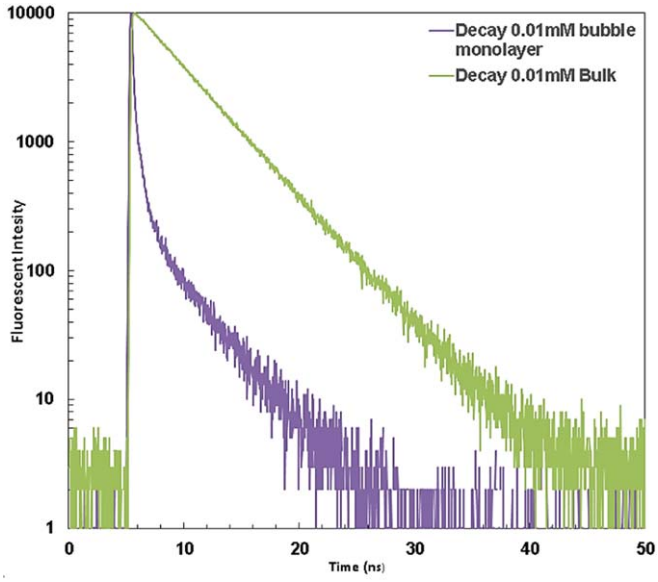


**Figure 9.** Fluorescence emission (560 nm) lifetime for 0.01 mM bulk solution and 0.01 mM bubble monalayer.

the shortening of lifetime (table S1 in supplementray material is available online at stacks.iop.org/JPENERGY/1/015007/mmedia). The first two fitted decay parameters from the monolayer emission curve are very short (range of 0.47–0.1 ns) in comparison to third decay component, which is 3.54 ns. Three different lifetime confirms the presence of three different species. The bulk liquid emission decay curve was fitted to single parameter with 4.25 ns lifetime, which is consistent with the value of Rh 6 G in water [49]. The longer lifetime is related to monomer whereas the shorter decay components indicates the formation of the agglomerate and interaction with dye molecules [26]. The dye concentration increases through enhanced adsorption if the gap between bubbles decreases. The short range attractraction promotes the dye agglomeration due to higher concentration. The results show that the decay of the stimulated emission is multiexponential.

## 6. Conclusion

A high threshold stimulated emission centred at 595 nm wavelength was shown to occur at the interface between two neighbouring bubbles in Rhodamine 6G-doped foams excited with a 532 nm laser. The stimulated emission was highly dependent on the laser incidence angle, the gap between two adjacent bubbles rather than the diameter of the bubbles. Additionally, the liquid fraction of the foam is a key factor for channelling photons at the interfaces. An efficient reflection and the use of reflective surfaces as substrates are crucial for obtaining single model stimulated light amplification for high loss foam systems. This can, however, be useful for efficient light guiding. The foam can be used as a template for adsorbed nanoparticles and dyes to create a highly regular structure of nanoparticles at a low cost. A 2D structure with a regular array of hole can be stacked in *z*-direction to create a 3D structure capable of absorbing multiphoton for an increased catalytic reaction.

## Acknowledgments

The authors are grateful for the support of EPSRC grant 'Photo-catalytic bubble reactor for conversion of $CO_2$ to fuels' EP/J02161X/1. The authors are also grateful to Professor. Girkin, Durham University for useful discussions. We thank EPSRC for support through the loan of the laser system and spectrophotometer. The authors also thank Mohammed Alamiry for experimental work and spectroscopic data collection and Dr Graham Hungerford for assisting to use a transient measurement system at Horiba Scientific, Glasgow, UK. Supporting data are openly available on Robert Gordon University's research portal (https://openair.rgu.ac.uk/handle/10059/1385).

## ORCID iDs

Ketan Pancholi https://orcid.org/0000-0001-7662-7764
Peter K J Robertson https://orcid.org/0000-0002-5217-661X

## References

[1] Fiabane J, Prentice P and Pancholi K 2016 High yielding microbubble production method *BioMed. Res. Int.* **2016** 3572827
[2] Malik R, Pancholi K and Melzer A 2016 Microbubble–liposome conjugate-payload evaluation of potential theranostic vehicle *Nanobiomedicine* **3** 1–8
[3] Nam Y S, Shin T, Park H, Magyar A P, Choi K, Fantner G, Nelson K A and Belcher A M 2010 Virus-templated assembly of porphyrins into light-harvesting nanoantennae *J. Am. Chem. Soc* **132** 1462–3
Zada I, Zhang W, Zheng W, Zhu Y, Zhang Z, Zhang J, Imtiaz M, Abbas W and Zhang D 2017 The highly efficient photocatalytic and light harvesting property of Ag-$TiO_2$ with negative nano-holes structure inspired from cicada wings *Sci. Rep.* **17277** 7
[4] Beattie N S, Zoppi G, See P, Farrer I, Duchamp M, Morrison D J, Miles R W and Ritchie D A 2014 Analysis of InAs/GaAs quantum dot solar cells using Suns-Voc measurements *Sol. Energy Mater. Sol. Cells* **130** 241–5
[5] Adams M, Skillen N, McCullagh C and Robertson P K J 2013 Development of a doped titania immobilised thin film multi tubular photoreactor *Appl. Catal.* B **130** 99–105
[6] Biswas S, Ahn H-Y, Bondar M V and Belfield K D 2012 Two-photon absorption enhancement of polymer-templated porphyrin-based J-aggregates *Langmuir* **28** 1515–22
[7] Narayanan L, Wooyul K and Wonyong C 2008 Effect of the agglomerated state on the photocatalytic hydrogen production with in situ agglomeration of colloidal $TiO_2$ nanoparticles *J. Phys. Chem.* C **112** 20451–7
[8] Bian Z, Tachikawa T and Majima T 2012 Superstructure of $TiO_2$ crystalline nanoparticles yields effective conduction pathways for photogenerated charges *J. Phys. Chem. Lett.* **3** 1422–7
[9] Stolarczyk J K, Bhattacharyya S, Polavarapu L and Feldmann J 2018 Challenges and prospects in solar water splitting and $CO_2$ reduction with inorganic and hybrid nanostructures *ACS Catalysis* **8** 3602–35
[10] Hanczyc P, Sznitko L, Zhong C and Heeger A 2015 Stimulated emission from Rhodamine 6G aggregates self-assembled on amyloid protein fibrils *ACS Photonics* **2** 1755–62
[11] Cachoncinlle C, Millon E, Petit A and Nistor M 2017 Random Lasing in wide-gap semiconductor thin films under deep UV pulsed laser pumping *Mater. Today: Proc.* **4** S52–61
[12] Peyvast N, Zhou K, Hogg R A and Childs D T D 2016 Dominant role of many-body effects on the carrier distribution function of quantum dot lasers *Appl. Phys. Express* **9** 032705
[13] Ye L, Kang J, Yang H, Liu B, Hu Z, Zu Y, Liu Y and Cui Y 2016 Enhancement of random lasing assisted by Ag nanoparticle doped dye medium in solidified fiber *Laser Phys.* **26** 045001
[14] Heydari E, Pastoriza-Santos I, Liz-Marza´n L M and Stumpe J 2017 *Nanoscale Horiz.* **2** 261
[15] Shibaev V P and Bobrovsky A Y 2017 Liquid crystalline polymers: development trends and photocontrollable materials *Russ. Chem. Rev.* **86** 1024
[16] Sreekanth P, Piccardi A, Raouf B, Buchnev O, Kauranen M, Strangi G and Assanto G 2018 Beaming random lasers with soliton control *Nat. Commun.* **3863** 9
[17] Lahoz F, Martín I R, Urgellés M, Marrero-Alonso J, Marín R, Saavedra C J, Boto A and Díaz M 2015 *Laser Phys. Lett.* **12** 045805
[18] Zeng H, Cai W, Liu P, Xu X, Zhou H, Klingshirn C and Kalt H 2008 ZnO-based hollow nanoparticles by selective etching: elimination and reconstruction of metal−semiconductor interface, improvement of blue emission and photocatalysis *ACS Nano* **2** 1661–70
[19] Wiersma D S 2008 The physics and applications of random lasers *Nat. Phys.* **4** 359
[20] Lagendijk A, van Tiggelen B and Wiersma D S 2009 Fifty years of anderson localization *Phys. Today* **62** 24–9

[21] Milner V and Genack A Z 2005 Photon localization laser: low-threshold lasing in a random amplifying layered medium via wave localization *Phys. Rev. Lett.* **94** 073901
[22] Cyprych K, Kopczyn´ska Z, Kajzar F, Rau I and Mysliwiec J 2015 Tunable wavelength light emission and amplification in Rhodamine 6G aggregates *Adv. Device Mater.* **1** 69–73
[23] Bhattacharya S and Mandal S S 1997 Interaction of surfactants with DNA. Role of hydrophobicity and surface charge on intercalation and DNA melting *Biochim Biophys. Acta.* **1323** 29–44
[24] Shyamal M, Mazumdar P, Maity S, Samanta S, Sahoo G P and Misra A 2016 Highly selective turn-on fluorogenic chemosensor for robust quantification of Zn (II) based on aggregation induced emission enhancement feature *ACS Sensors* **1** 739–47
[25] Kikteva T, Star D, Zhao Z H, Baisley T L and Leach G W 1999 Molecular orientation, aggregation, and order in Rhodamine films at the fused silica/air interface *J. Phys. Chem.* B **103** 1124–33
[26] Fedoseeva M, Letrun R and Vauthey E 2014 Excited-state dynamics of Rhodamine 6G in aqueous solution and at the dodecane/water interface *J. Phys. Chem.* B **118** 5184–93
[27] Schmiedeberg M, Miri M and Stark H 2005 Photon channelling in foams *Eur. Phys. J.* E **18** 123–31
[28] Whitesides G M 2006 The origins and the future of microfluidics *Nature* **442** 368–73
[29] Bog U, Laue T, Grossmann T, Beck T, Wienhold T, Richter B, Hirtz D M, Fuchs H, Kalt H and Mappes T 2013 On-chip microlasers for biomolecular detection via highly localized deposition of a multifunctional phospholipid ink *Lab Chip* **13** 2701
[30] Pancholi K, Farook U, Moaleji R, Stride E and Edirisinghe M 2008 Novel methods for preparing phospholipid coated microbubbles *Eur. Biophys. J.* **37** 515–20
[31] Gittings A S, Bandyopadhyay R and Durian D J 2004 Photon channelling in foams *Europhys. Lett.* **65** 414–9
[32] Vezenov D V, Mayers B T, Wolfe D B and Whitesides G M 2005 Integrated fluorescent light source for optofluidic applications *Appl. Phys. Let.* **86** 041104
[33] Swathi M G and Ahipa T N 2018 Aggregation induced emission properties of new cyanopyridone derivatives *J. Mol. Liq.* **265**
[34] Ivanov I B 1988 *Surfactant Science Series* vol 29 (New York: Mercel Dekker Incl)
[35] Melnikau D, Savateeva D, Chuvilin A, Hillenbrand R and Rakovich Y 2011 'Whispering gallery mode resonators with J-aggregates' *Opt. Express* **19** 22280–91
[36] Tajalli H, Ghanadzadeh Gilani A, Zakerhamidi M S and Moghadam M 2009 Effects of surfactants on the molecular aggregation of Rhodamine dyes in aqueous solutions *Spectro. Acta* A **72**
[37] Hecht E and Zajac A 2000 *Optics* 4th Edn (Reading, MA: Addison-Wesley)
[38] Tchoukov P, Mileva E and Exerowa D 2003 Experimental evidences of self-assembly in foam films from amphiphilic solutions *Langmuir* **19** 1215–20
[39] Vessely C R, Carpenter J F and Schwartz D K 2005 Calcium-induced changes to the molecular conformation and aggregate structure of â-casein at the air–water interface *Biomacromolecules* **6** 3334–44
[40] Leonetti M and Lopez C 2014 Modes structures and interaction in random lasers *Light Localisation and Lasing: Random and Pseudo-random Photonic Structures* ed M Ghulinyan and L Pavesi (Cambridge: Cambridge University Press)
[41] Salleres S, López Arbeloa F, Martínez V, Corcóstegui C and López Arbeloa I 2009 Effect of surfactant C12TMA molecules on the self-association of R6G dye in thin films of laponite clay *Mater. Chem. Phys.* **116** 550–6
[42] Aviv H, Harazi S, Schiff D, Ramona Y and Tischler Y R 2014 Synthesis of an amphiphilic Rhodamine derivative and characterization of its solution and thin film properties *Thin Solid Films* **564** 86–91
[43] Sun Q and Hutzler S 2007 Light scattering through 2D Plateau borders and foams *Colloids Surf.* A **309** 1–3
[44] Sadjadi Z, Miri M and Stark H 2008 Diffusive transport of light in three-dimensional disordered Voronoi structures *Phys. Rev.* E **77** 051109
[45] Vera M U, Saint-Jalmes A and Durian D J 2001 Scattering optics of foam *Appl. Opt.* **40** 4210–4
[46] Yuan Y, Li X and Tu J 2018 Effects of spontaneous nanoparticle adsorption on the bubble-liquid and bubble-bubble interactions in multi-dispersed bubbly systems–a review *Int. J. Heat Mass Transfer* **120** 552–67
[47] Laube J, Baric V, Salameh S, Mädler L and Colombi Ciacchi L 2018 A new contact model for the discrete element method simulation of $TiO_2$ nanoparticle films under mechanical load *Granular Matter* **28** 20
[48] Casperson L W 1977 Threshold characteristics of mirrorless lasers *J. Appl. Phys.* **48** 256–62
[49] Quentin S, Hanley Vinod Subramaniam Donna J and Arndt-Jovin Thomas M J 2001 Fluorescence lifetime imaging: multi-point calibration, minimum resolvable differences, and artifact suppression *Cytometry* **43** 248–60